Geochimica et Cosmochimica Acta 393 (2025) 208–218

Contents lists available at ScienceDirect

Geochimica et Cosmochimica Acta

journal homepage: www.elsevier.com/locate/gca

Chlorine and NaCl in hydrous basaltic melts

Monika K. Rusiecka *, Bernard J. Wood

Department of Earth Sciences, University of Oxford, South Parks Road, Oxford OX1 3AN UK

ARTICLE INFO

Associate editor: Fabrice Gaillard

Keywords:
Cl solubility in melts
Chloride capacity
NaCl activity in melts
Fluid salinity
Basalt

ABSTRACT

We have determined the solubility and behavior of chlorine in hydrous basaltic melts at high pressures (0.5–1.5 GPa) and temperatures (1200–1300 °C) using the chlorine fugacity control method of Thomas and Wood (2021). By systematically increasing the water content of the melt from 0 to 4 wt% at fixed chlorine and oxygen fugacities we find that addition of H_2O leads to an increase in chlorine concentration under all conditions studied. In order to develop a comprehensive equation for chlorine solubility we combined our data with 60 results on anhydrous compositions from Thomas and Wood (2021,2023). We define chloride capacity C_{Cl} for each experiment as:

$$C_{Cl} = \frac{Cl(wt.\%)}{\sqrt{fCl_2}} \times \sqrt[4]{fO_2}$$

The 70 results were then fitted by stepwise linear regression to an equation containing pressure, temperature and compositional terms. Terms which did not pass the F-test ($\alpha = 0.05$) were excluded. This approach led to the following fit-equation, with P in GPa and X_{Si} X_{Ca} referring to mole fractions of the oxides on a single cation basis:

$$logC_{Cl} = 1.492 + \frac{4331X_{Ca} - 3508X_{Si} + 2440X_{Fe} - 3921X_K - 741P}{T}$$

The standard error of the fit is 0.083 and R^2 is 0.963. This equation closely approximates that obtained from the results on anhydrous compositions by Thomas and Wood (2023). Surprisingly the term in $HO_{0.5}$ was found not to be significant, implying that water behaves as an ideal diluent with respect to chlorine.

We used our chloride capacity equation to calculate the activity of NaCl in experimentally-produced hydrous basalts of known chlorine content. The method involved combining chloride capacities with Na_2SiO_3 and SiO_2 activities derived from the Rhyolite-MELTS program. The results for NaCl activity were found to be in reasonably good agreement with values obtained from the Thomas and Wood (2023) equation which had been based predominantly on data from silica-rich compositions. Finally, measurements of the compositions of melt inclusions from Etna were used to calculate the activities of NaCl in the inclusions and the salinities of fluids with which the inclusions would be in equilibrium. From the trapping pressures of the inclusions and their compositions we find that decompression from 500 MPa to ~50 MPa is accompanied, in this case, by a salinity increase from <1 wt% NaCl to ~50 % NaCl.

1. Introduction

In silicate melts, H_2O and CO_2 are the two volatile components whose solubilities and behaviour are best understood (Symonds et al., 1994; De Vivo et al., 2005). In the case of H_2O, this is due to its commonly high abundance, the major effects it has on melting and crystallisation temperatures of melts, and its importance in high temperature hydrothermal ore deposition. The significance of CO_2 became evident with the development of accurate methods of collection and analysis of volcanic gases (Gerlach and Nordlie, 1975; Heald et al., 1963a,b). Such volcanic gases have been recognised as important contributors to the budget of "greenhouse" CO_2 in the atmosphere and this has led to the development of an extensive database to describe CO_2 solubility in a broad spectrum of melts over a wide range of physical conditions (Brooker et al. 2001; Stanley et al. 2011). The solubility data for H_2O and CO_2 have also been developed into generally applicable models such as *H2OSOL* (Moore et al., 1998) *VolatileCalc* (Newman and Lowenstern, 2002) and *MagmaSat* (Ghiorso and Gualda, 2015).

Due to their significant abundances in volcanic gases and sensitivity to redox conditions sulfur species in melts have also received considerable attention. In silicate melts sulfur dissolves, depending on oxygen fugacity, either as S^{2-} or S^{6+} (Fincham and Richardson, 1954). In

* Corresponding author.
E-mail address: monika.rusiecka@earth.ox.ac.uk (M.K. Rusiecka).

https://doi.org/10.1016/j.gca.2025.01.020
Received 28 August 2024; Accepted 16 January 2025
Available online 23 January 2025

volcanic gases it occurs primarily as SO_2 or H_2S. Recent experimental work at 1 atm pressure has precisely defined the temperature-composition-fO_2 dependences of S^{2-} and S^{6+} solubility and stability in silicate melts (Boulliung and Wood, 2022, 2023; O'Neill and Mavrogenes, 2022; O'Neill and Mavrogenes, 2002). These data enable accurate prediction of sulfur degassing behaviour and associated redox changes under crustal conditions (Boulliung and Wood, 2023; Ding et al., 2023) and facilitate the development of complex melt-fluid degassing models (Ding et al., 2023).

As implied above volcanic gases normally comprise more than 90 % H_2O plus CO_2, with lesser amounts (<10 %) of SO_2 and H_2S. They also contain significant amounts of the halogens Cl and F as HCl and HF, together with trace amounts of HBr and HI (Pyle and Mather, 2009; Martin et al., 2012). During cooling and differentiation, the halogens behave as highly incompatible elements (Edmonds et al., 2009; Pyle and Mather, 2009) and are generally concentrated in the melt until separation of a gas or fluid into which they are strongly partitioned. Current degassing from volcanicity is estimated to emit up to 5.5 Tg/yr of HCl, and between 0.15 Tg/Yr and 0.58 Tg/yr of HF with much smaller amounts of HBr and HI (Gerlach 2004; Aiuppa et al., 2009; Pyle and Mather, 2009; Webster et al., 2018). The released halogens, particularly Cl, transport trace metals in gaseous form into the environment (e.g., Cu, Cd, Pb, Scholtysik and Canil, 2021), act as catalysts for the destruction of stratospheric ozone (von Glasow et al., 2009), and in some cases can cause major local environmental degradation. For example, a large amount of F (~8 million tonnes) was released from the 1783 eruption of Laki in Iceland. These emissions led to the deaths of a large fraction of Iceland's sheep and cattle population and an ensuing famine in the human population. Chlorine, similar in abundance to F (~30 ppm) in the silicate Earth (Palme and O'Neill, 2013) is a significant ligand in hydrothermal processes and plays a major role in transporting economically important metals such as Au and Cu in aqueous solution (Blundy et al., 2015). Major economic deposits at, for example, Broken Hill in New South Wales, Australia (Millsteed and Mavrogenes, 2015) and various porphyry copper deposits (Nash, 1976; Fuge et al., 1986) have been found to be associated with NaCl-rich fluid inclusions. The deposits arise from segregation of Cl-rich brines from melts in the later stages of igneous activity, the economically important metals being transported as chloride complexes in solution. Halite-rich fluid inclusions, also outline the Cu-rich ore zone at Bingham Canyon, Utah, USA (Moore and Nash, 1974) and are associated with the two most economically important iron oxide copper–gold (IOCG) deposits in Chile, Mantoverde, and Candelaria-Punta del Cobre, (Marschik and Kendrick, 2015).

The properties and distribution of halogens in natural and experimentally produced silicate melts and fluids are, given their environmental, economic and geochemical importance, the subject of broad interest. Halogens have profound effects on the phase equilibria and viscosities of melts (Zimova and Webb, 2006; Filiberto and Treiman, 2009; Baasner et al., 2013) leading, for example, to Cl being twice as effective on a molar basis at lowering the liquidus temperature of basalt as H_2O (Filiberto and Treiman, 2009). Experimental data indicate that Cl solubility increases with decreasing SiO_2 concentration and with corresponding increases in network-modifying cations such as CaO in the melt (Signorelli and Carroll, 2000; Thomas and Wood, 2023; Webster and De Vivo, 2002). In an attempt to quantify these compositional effects Webster et al. (2015) performed experiments in which silicate melts were saturated in hydro-saline liquids under known pressure–temperature conditions. The data were parameterized as a Cl solubility model which incorporates the compositional effects of CaO, MgO and alkalis (Webster et al., 2015). Although an important step forward, this model retains significant uncertainties because of the lack of constraints on chlorine fugacity and NaCl activity. Our aim here is to develop such constraints for chlorine and NaCl behaviour in hydrous basalts.

Thomas and Wood, (2021) proposed an approach to buffering chlorine fugacity in silicate melts using a modification of a well-known experimental technique (Frantz and Eugster, 1973). This relies on the fact that Ag has very low solubility in silicate melts so fugacities of the halogens can be controlled using mixtures of their silver salts with metallic silver.

$$AgCl_{(liquid)} = 2Ag_{(liquid)} + Cl_{2(gas)} \quad (1)$$

Coexistence of liquid AgCl and liquid Ag metal at fixed pressure and temperature buffer the fugacity of Cl_2. In theory, the composition of a coexisting silicate melt can be varied almost at will at a known, buffered, chlorine fugacity with minimal dissolution of Ag. In practice chlorine fugacities are so high using the Ag/AgCl buffer that discrete Ca-Mg chloride liquids tend to segregate modifying the compositions of haplobasaltic melts. In order to suppress the segregation of chlorides, the AgCl is mixed with AgI to form a mixed halide with a known ratio of Cl to I. This approach enables the Cl_2 fugacity to be calculated from a combination of the thermodynamic data for equilibrium (1), the volumes of the liquid Ag and AgCl, and the ratio of Cl/(Cl + I) in the "sliding" Ag/AgCl-AgI buffer. It also enables the effect of varying Cl_2 fugacity at fixed pressure and temperature to be measured by changing the AgI/AgCl ratio. Iodine behaves like Ag in that it is virtually insoluble (~ 0.1 wt%) in all of the silicate melts investigated to date (Thomas and Wood, 2021, 2023).

In their initial study Thomas and Wood, (2021) used the Ag/AgCl buffer method to study Cl dissolution behaviour in an Icelandic basalt and a haplobasalt of composition $An_{50}Di_{28}Fo_{22}$. At 1.5 GPa/1400 °C, dissolution of Cl was found to obey Henry's Law with the Cl concentration proportional to the square root of Cl_2 fugacity and the fourth root of oxygen fugacity up to at least 1.6 wt% Cl in the basalt and 2.6 wt% Cl in the haplobasalt. These observations indicate that $2Cl^-$ ions in the melt replace O^{2-} according to the reaction:

$$Cl_{2(gas)} + \left[O^{2-}\right]_{melt} = 2\left[Cl^-\right]_{melt} + \frac{1}{2}O_{2(gas)} \quad (2)$$

If Cl^- ions in the melt are dissociated from one another it is straightforward to show that, at equilibrium, the concentration of Cl^- in the melt is proportional to $f_{Cl_2}^{0.5}$ and inversely proportional to $f_{O_2}^{0.25}$ as observed.

In a second study using the AgCl/Ag method of controlling chlorine fugacity Thomas and Wood (2023) measured the effect of composition on chloride capacities of silicate melts. They defined chloride capacity C_{Cl} for a melt of fixed major element composition as follows:

$$C_{Cl} = \frac{Cl(wt.\%)}{\sqrt{fCl_2}} \times \sqrt[4]{fO_2} \quad (3)$$

Experimental data on 25 different compositions, predominantly at 1.5 GPa/1400 °C when combined with the earlier results at different temperatures and pressures led to:

$$logC_{Cl} = 1.601 + (4470X_{Ca} - 3430X_{Si} + 2592X_{Fe} - 4092X_K - 894P)/T. \quad (4)$$

In this equation X_{Ca}, X_{Si} refer to the mole fractions of the oxides of the subscript elements on a single cation basis, P is the pressure in GPa and T is temperature K. Equation (4) fits the chloride capacity data (60 points) with an r^2 of 0.96 and a standard error of 0.089 (Thomas and Wood, 2023). It also highlights the strong influence of CaO on chloride capacity, an influence that is implicit in results of nuclear magnetic resonance spectroscopy on quenched glasses (Sandland et al., 2004; Stebbins and Du, 2002) and explicitly incorporated in the chlorine solubility model of Webster et al (2015). A more recent EXAFS (Extended X-Ray Absorption Fine Structure) study of Cl-bearing glasses (Thomas and Wood, 2023) found changes in the Cl spectrum linked to concentrations of Ca, Mg, Fe and Na in the glass. This suggests, in agreement with equation (4), that these major elements affect Cl bonding and hence Cl thermodynamic properties in melts.

Chlorine behaviour in silicate melts must, of course depend on the behaviour of the fluid phases which are released in the later stages of magmatism. This leads to two important questions. Firstly, is the chloride capacity of a melt dependent on the concentration of H_2O and if so, what is the dependence? Secondly, how does the chlorine content of the melt affect the activity of NaCl and other chloride species in the melts and the fluids they release?

Thomas and Wood (2023) addressed the first of these questions by using 23 experimental data points on Cl partitioning between hydrous phonolite and fluid at pressures below 0.2 GPa (Alletti et al., 2014) to show that H_2O contents up to 4.3 wt% should have little effect on chloride capacity. Use of the data required a number of assumptions about speciation in the fluid, however so this conclusion was only provisional. In order to address the second question about NaCl activity, Thomas and Wood (2023) performed experiments in which anhydrous phonolite melt was saturated in NaCl at 1GPa/1100 °C. These yielded compositions of silicate melts at NaCl activity of 1.0. These were combined with 100 data points from Webster and De Vivo (2002) and Webster et al (2015) in which silicate melts were saturated in hydrosaline NaCl-KCl melts at 0.1 to 700 MPa and temperatures of 700 to 1250 °C. Because the compositions of the hydrosaline melts were not given in the latter studies, Thomas and Wood assumed a constant NaCl activity of 0.8 for these points. The combined dataset was used to derive pressure–temperature-compositional effects on NaCl activity:

$$\log(\mathrm{Cl}) = \log(a_{NaCl}) + 0.06 - (2431X_{Ca} + 3430X_{Si} - 2592X_{Fe} + 3484X_{Na} + 4092X_{K} - 2417)/T. \quad (5)$$

X_{Ca} X_{Si} refer to the mole fractions of CaO and SiO_2 with all mole fractions on a single cation basis and (Cl) is the chlorine content of the melt in weight %. Although equation (5) fits the data reasonably well, with r^2 of 0.85 and standard error of 0.124, the data do not provide any useful constraints on the effects of H_2O content of the melt on NaCl activity.

In summary, given the importance of Cl in transporting metals in both hydrothermal solutions and in volcanic gases our goals are to determine the influence of H_2O, the major component of such gases and fluids on the behaviour of Cl in silicate melts. The first part of the study involves measurements of the chloride capacities of hydrous melts at fixed chlorine and oxygen fugacities as H_2O content increases. The second goal is to determine the effects of H_2O dissolved in the silicate melt on the activity of NaCl and the partitioning of NaCl into the brine which coexists with and segregates from the melt.

2. Experimental procedure

A series of experiments was conducted using starting material with the composition of basalt from Reykjanes Ridge, Iceland (Norris and Wood, 2017, Thomas and Wood 2021, 2023). Three powders were prepared with three different water contents. The starting materials were prepared from mixtures of analytical grade oxide (SiO_2, TiO_2, MgO, Al_2O_3, $Fe_{0.95}O$) and carbonate (Na_2CO_3, $CaCO_3$) powders. Powders were ground under ethanol for 2 h. Then the mixtures were decarbonated overnight by heating from 400 to 800 °C at the rate of 2 °C/min. Water was added as $Al(OH)_3$ and iron was added as $Fe_{0.95}O$ after the powders were decarbonated. Next the powders were ground again under ethanol for at least 2 h. A small fraction of each powder was melted at 1400 °C in air at 1 atm to verify the starting composition. A small fraction of each powder was also placed in an $Au_{80}Pd_{20}$ capsule and melted at 1.5 GPa and 1300 °C to check water contents (Table 1). The starting composition and water contents were verified using EPMA.

Chlorine fugacity was controlled by mixing AgI and AgCl in 80:20 proportion following the procedure developed by Thomas and Wood (2021). The fugacity of Cl can then be obtained from Thomas and Wood (2021) as (pressure in GPa):

$$\log f_{Cl_2} = -\frac{1140}{T} + 2.961 + 2150\frac{P}{T} - 208\frac{P^2}{T} + 2\log\left[\frac{Cl}{Cl+I}\right]_{halide} - 2log\left[\frac{Ag}{Ag+Pt}\right]_{metal} \quad (6)$$

The starting silicate compositions were ground with the AgI/AgCl buffer in the buffer:silicate ratio of 75:25 and packed into 2.5 mm OD (outer diameter) and 1 mm ID (inner diameter) graphite capsules. The graphite capsules were placed together with a graphite lid on top of a layer of Ag_2CO_3 in a 3 mm OD Pt capsule. During the experiment the Ag_2CO_3 decomposes to metallic Ag, CO_2 and O_2 which buffers the oxygen fugacity at, or close to (depending on H_2O content), the CCO buffer. The Pt capsule was placed in a 4 mm OD $Au_{80}Pd_{20}$ capsule which was packed with the starting silicate material mixed with graphite (Figure in supplementary information).

The experiments were conducted in an end-loaded ½ inch piston cylinder apparatus at the University of Oxford. At 1.0 and 1.5 GPa CaF_2 was used as the pressure medium while the experiments conducted at 0.5 GPa used the NaCl-borosilicate glass assembly. The 4 mm OD $Au_{80}Pd_{20}$ capsule was placed in the centre of the graphite furnace in a pyrophyllite outer sleeve with crushable MgO pieces above and below the capsule. Temperature was controlled by an alumina-sheathed C-type thermocouple (at 1.0 and 1.5 GPa) and by a mullite-sheathed welded S-type thermocouple (at 0.5 GPa) introduced through a hole in the MgO piece above the capsule and separated from the capsule by a 0.5 mm thick alumina disc.

3. Analytical procedures

The experimental run product capsules were placed in epoxy resin and ground to expose the charge inside the inner graphite capsules. The samples were ground and polished using baby oil as a lubricant and oil-based diamond suspensions to avoid chlorine loss. The charge was composed of glass, Ag-rich metal blobs and a metal chloride-iodide phase. The silicate glasses, metal chloride-iodide phase and the metal blobs were analysed using the CAMECA SXFive-FE electron microprobe at the Department of Earth Sciences, University of Oxford. An accelerating voltage of 15 kV, 4nA beam current and a 20 μm defocused beam was used for the analyses of the glass and chloride-iodide and 15 kV, 20nA beam current and a 1 μm focused beam was used to analyse the metal blobs. The standards used were albite (Si, Al, Na), wollastonite (Ca), fayalite (Fe in the glass phase), elemental Fe (Fe in metal and chloride-iodide), thallium bromoiodide (I), sanidine (K), periclase (Mg), TiO_2, elemental Ag and Pt, and high purity synthetic NaCl crystals (Cl). Secondary standards used were St. John's Island olivine and labradorite crystals. Counting times were 30 s on the peak and 15 s on the background for most elements except Cl (60 s peak and 30 s background), Mg (40 s peak and 20 s background) and Na (20 s peak and 10 s background).

The concentrations of H_2O and CO_2, together with Si and Mg were analysed in 5 samples mounted in 2 gold-coated epoxy mounts using the

Table 1
Chemical composition of the starting materials on anhydrous basis.

	SiO_2	TiO_2	Al_2O_3	FeO	MgO	CaO	Na_2O	K_2O	H_2O
ICB-2	50.66 ± 0.26	1.01 ± 0.03	14.42 ± 0.18	9.74 ± 0.13	9.23 ± 0.09	12.73 ± 0.14	2.15 ± 0.11	0.05 ± 0.02	2.67 ± 0.45
ICB-4	50.68 ± 0.22	1.02 ± 0.03	14.06 ± 0.14	9.75 ± 0.14	9.36 ± 0.08	12.87 ± 0.10	2.17 ± 0.12	0.08 ± 0.03	4.38 ± 0.41
ICB-8	51.41 ± 0.23	1.01 ± 0.04	13.20 ± 0.13	9.61 ± 0.13	9.46 ± 0.10	12.93 ± 0.19	2.31 ± 0.10	0.06 ± 0.02	6.29 ± 0.33

Cameca IMS-7f GEO at the NERC Ion Microprobe Facility at the University of Edinburgh. A primary beam of $^{16}O^-$ ions with a beam current of 5nA and an impact energy of 18 kV was used for a spot size of ~ 10 μm. Raw counts of ^{1}H, ^{12}C and ^{26}Mg were normalised to the rate count of ^{30}Si. Normalized count rates were converted into H_2O and CO_2 contents using calibration curves produced from analyses of well-characterised standards (N72, M47, M10, M5, M21, M36, M40, Shishkina et al. 2010, and 519–4-1, Hauri, 2002). The H_2O contents of the remaining samples were estimated by difference from EPMA analyses using the samples analysed by SIMS and a set of anhydrous samples of the same compositions as the starting materials as standards (Table 2). The CO_2 content was assumed to be uniform at each pressure based on the results of SIMS analyses (Table 2). Further details of the analyses can be found in the Supplementary material.

4. Results

Ten experiments were conducted using the hydrous Icelandic basalt at 3 different pressures (0.5, 1, and 1.5 GPa). The experiments at 0.5 and 1 GPa were performed at 1200 °C in order to minimize the diffusion of hydrogen out of the capsule and consequent water loss. The experiments conducted at 1.5 GPa and 1200 °C resulted in partial crystallization of the melt and therefore experiments at 1.5 GPa were conducted at 1300 °C. All experiments were performed with the same starting AgI to AgCl ratio and the same buffer to silicate ratio. Decreases, relative to the starting compositions, in the Na contents of the product glasses (Table 2) are, we believe, due to Na dissolution in the AgI/AgCl buffer. A typical reduction in Na_2O content of the glass from 2.15 % to 1.15 % would, however only reduce the Ag/(Ag + Na) ratio of the buffer from 1 to 0.98 thereby raising chloride capacity by the insignificant factor of 1.02. This is well within our experimental uncertainty and has been neglected. The oxygen fugacity was buffered close to C-CO-CO_2 (CCO) by coexistence of graphite with a predominantly C-O fluid phase. Shifts in fO_2 away from CCO due to the presence of H_2O were estimated from the H_2O activity.

At 1.0 and 1.5 GPa we used the equation of Jakobsson and Oskarsson (1994) to calculate the oxygen fugacity at the experimental conditions. Because this equation was only calibrated down to 0.75GPa, however we used a Modified Redlich Kwong (MRK) equation of state (Holloway, 1977) to calculate oxygen fugacity at 0.5 GPa. In this case we assumed the fluid was composed entirely of CO and CO_2 and that these were in equilibrium with the graphite capsule. We checked our MRK equation of state for CO-CO_2 mixtures in equilibrium with graphite by calculating fO_2 under the same conditions as Jakobsson and Oskarsson's experimental measurements. For this calculation we took 1 bar free energy data for CO and CO_2 from NIST-JANAF Tables and extrapolated them to high pressure using the Holloway (1977) version of the MRK equation. In order to obtain oxygen fugacity with the usual, 1 bar standard state, we applied the MRK mixing rules for CO-CO_2 mixtures (Holloway, 1977) and calculated fO_2 from each of the equilibria:

$$C(graphite) + O_2 = CO_2$$

$$2C(graphite) + O_2 = 2CO$$

The calculations used the molar volume of graphite of 5.288 cm^3 at 298 K, extrapolated to 1300 °C at 1 bar using thermal expansion data (Zhao et al., 2022) and integrated to experimental pressure using a constant compressibility of 0.034 GPa^{-1}(Hanfland et al., 1989). The mole fractions of CO and CO_2 in the CO-CO_2 mixture were adjusted until graphite, CO and CO_2 were all in equilibrium at the same oxygen fugacity. At 1.0 and 1.5 GPa our MRK calculation is within 0.05 logfO_2 units of the experimental results, indicating that we can be confident in our use of the MRK equation at 0.5 GPa. For hydrous experiments we used the equation of Moore et al (1998) to convert the H_2O contents of product glasses into fugacities of H_2O. Our MRK equation was then used to convert this fugacity into a mole fraction of H_2O and to calculate the mole fractions, fugacity coefficients and fugacities of CO, CO_2, H_2O, H_2 and CH_4 at the approximate fO_2 of the experiment. Finally, the computed CO and CO_2 fugacity coefficients and mole fractions were used to calculate fO_2 at graphite saturation with the given mole fraction and fugacity of H_2O. The effects of H_2O on fO_2 are small. At 1.5GPa and 1300 °C the maximum measured H_2O content (3.92 %, Table 2) lowers fO_2 by 0.03 log units relative to the anhydrous system. At 0.5 GPa the maximum H_2O content in the melt (3.18 %) lowers fO_2 by 0.18 log units relative to the dry case. Experiments at 1GPa shift in fO_2 by an amount intermediate between these two end-members. All reported fO_2 values in Table 2 have been corrected for H_2O content of the melt.

Fig. 1 shows the relationship between the water content and the chlorine content of the melt at 0.5, 1.0 and 1.5 GPa. Results are compared with the anhydrous data of Thomas and Wood (2021) which were recalculated to the same chlorine and oxygen fugacities as the hydrous experiments using equations (3) and (4). At fixed chlorine and oxygen fugacities chlorine contents increase approximately linearly with increasing water content to ~ 2 wt% H_2O and less dramatically in the range beyond 2 % H_2O. Additionally, chlorine content at constant buffer Cl/(I + Cl) increases with decreasing pressure (Fig. 1). All experimental conditions, Cl and water concentrations, oxygen and chlorine fugacities are given in Table 2.

Based on chlorine fugacities, oxygen fugacities and measured chemical compositions of the melts we determined chloride capacities as defined by eq. (3). When comparing our results with data for anhydrous compositions studied by Thomas and Wood (2021,2023), however, we noted a small error in their oxygen fugacities at 0.5 GPa. The latter were extrapolated linearly from the experimental range of 0.75–2 GPa and this extrapolation yields an apparent overestimate of oxygen fugacity at 0.5 GPa. The magnitude of the overestimate is 0.43 logfO_2 units at 0.5 GPa/1400 °C and 0.09 logfO_2 units at 0.5GPa/1100 °C. We therefore calculated oxygen fugacity at 0.5GPa using the MRK equation of state and corrected our oxygen fugacities and those of Thomas and Wood (2021, 2023) in order to refit the data and produce a revised equation for chloride capacity. First, we used only the anhydrous experiments of Thomas and Wood (2021, 2023) with corrected values of oxygen fugacity (60 points). We fitted the experimental logarithm of chloride capacity (eq. (3) to mole fractions calculated on a single cation basis using SPSS software. We used stepwise linear regression applying the F-test (α = 0.05) at each step and excluding any terms that were not significant at α = 0.05. This resulted in an equation for chloride capacity which is slightly modified from that of Thomas and Wood (2023):

$$logC_{Cl} = 1.512 + (4396X_{Ca} - 3446X_{Si} + 2568X_{Fe} - 4072X_K - 793P)/T. \quad (7)$$

$R^2 = 0.960$; standard error = 0.089 for 68 % confidence interval.

In equation (7), X_{Ca}, X_{Si} refer to mole fractions of the oxide on a single cation basis, P is pressure in GPa and T temperature K. We tested the applicability of this equation to hydrous systems by comparing it to the chlorine data of Fig. 1. Fig. 2 shows the experimental measurements of Fig. 1 plotted versus calculated values from our fit equation (7) without considering $HO_{0.5}$ in the sum of mol fractions i.e., the compositions were all recalculated to 100 % as if they were anhydrous. As can be seen, equation (7) slightly underestimates chloride capacities for most of our hydrous experiments if these are treated on an anhydrous basis. Fig. 3 shows an alternative approach. Here, our experimental measurements of the logarithm of chloride capacity (log(C_{Cl}) experimental) are plotted versus calculated values from our fit equation (7) (log(C_{Cl}) calculated) under the assumption that $HO_{0.5}$ is a simple diluent i.e., there is no $HO_{0.5}$ term in the fit equation and all mole fractions are applied to equation (7) with the true, measured values. As can be seen, with the assumption of $HO_{0.5}$ as an ideal diluent, equation (7) reproduces all of the hydrous data within experimental error.

We next tested our conclusion that $HO_{0.5}$ can be treated as an ideal diluent by adding our 10 hydrous experiments to the 60 anhydrous data (Thomas and Wood, 2021,2023) and fitting them using the same fitting procedure as before. This resulted in an equation for chloride capacity

Table 2
Experimental conditions and chemical compositions of the melt in each experiment.

	T (℃)	n	P (GPa)	fO_2	fCl_2	SiO_2	TiO_2	Al_2O_3	FeO	MgO	CaO	Na_2O	K_2O	H_2O	CO_2	Cl	initial Cl/(Cl + I)	final Cl/(Cl + I)	final Ag/(Ag + Pt)
AgI/Cl-023 (Thomas and Wood 2021) modified	1300	13	1.5	6.76E-08	1.84E-04	54.94 (±0.94)	0.95 (±0.05)	15.11 (±0.56)	3.24 (±0.89)	8.86 (±0.36)	12.3 (±0.45)	1.42 (±0.13)	0	0	0.9 (±0.02) *	0.8 (±0.1)			
ICB-1 (this study)	1300	43	1.5	1.10E-08	2.10E-04	51.17 (±0.86)	1.02 (±0.04)	14.55 (±0.38)	5.13 (±0.24)	9.28 (±0.30)	12.49 (±0.30)	1.37 (±0.20)	0.03 (±0.02)	1(±0.4) [2]	0.9 (±0.04) *	1.6 (±0.08)	0.29	0.27	0.98
ICB-2 (this study)	1300	21	1.5	1.10E-08	2.01E-04	48.4 (±0.76)	0.96 (±0.04)	12.7 (±0.44)	7.92 (±0.30)	8.92 (±0.32)	11.99 (±0.30)	1.24 (±0.18)	0.02 (±0.02)	1.21 (±0.06) [1]	0.9 (±0.04) [1]	2 (±0.08)	0.29	0.27	0.98
ICB-3 (this study)	1300	32	1.5	1.29E-08	1.95E-04	46.79 (±0.74)	0.95 (±0.06)	12.32 (±0.30)	7.74 (±0.28)	8.65 (±0.28)	11.71 (±0.34)	1.23 (±0.14)	0.03 (±0.02)	3.92 (±0.1) [1]	0.9 (±0.04) [1]	2.57 (±0.16)	0.29	0.26	0.98
AgI/Cl-048 (Thomas and Wood 2021) modified	1200	40	1	2.09E-08	2.00E-05	50.08 (±0.69)	0.93 (±0.05)	14.55 (±0.32)	7.58 (±0.17)	8.59 (±0.12)	11.93 (±0.12)	1.61 (±0.09)	0	0	0.4 (±0.02) *	2.03 (±0.1)			
ICB-4 (this study)	1200	28	1	4.92E-10	2.29E-05	48.39 (±0.1.42)	1.01 (±0.06)	13.78 (±0.40)	8.57 (±0.28)	8.79 (±0.44)	12.02 (±0.28)	1.03 (±0.14)	0.02 (±0.02)	1.94 (±0.4) [2]	0.4 (±0.04) *	2.64 (±0.06)	0.29	0.26	0.99
ICB-5 (this study)	1200	22	1	4.59E-10	2.27E-05	48.45 (±0.92)	1 (±0.06)	14.03 (±0.36)	8.46 (±036)	8.57 (±0.20)	11.79 (±0.36)	1.05 (±0.20)	0.02 (±0.02)	2.47 (±0.4) [2]	0.4 (±0.02) *	2.68 (±0.08)	0.29	0.26	0.99
ICB-6 (this study)	1200	41	1	3.89E-10	2.27E-05	48.28 (±0.72)	0.98 (±0.06)	13.26 (±0.32)	8.41 (±0.28)	8.45 (±0.28)	11.66 (±0.22)	1.06 (±0.16)	0.02 (±0.02)	3.75 (±0.4) [2]	0.4 (±0.02) *	2.85 (±0.08)	0.29	0.26	0.99
ICB-7 (this study)	1200	36	1	3.83E-10	2.25E-05	47.51 (±1.02)	0.98 (±0.06)	12.71 (±0.40)	8.13 (±0.34)	8.45 (±0.32)	11.72 (±0.28)	0.99 (±0.16)	0.02 (±0.02)	3.87 (±0.06) [1]	0.4 (±0.02) [1]	3.13 (±0.18)	0.29	0.26	0.99
ICB-8 (this study)	1200	37	0.5	7.31E-11	5.31E-06	49.6 (±1.08)	1.02 (±0.06)	13.59 (±0.38)	8.13 (±0.44)	8.97 (±0.32)	12.12 (±0.28)	0.79 (±0.14)	0.01 (±0.02)	1.41 (±0.04) [1]	0.1 (±0.02) [1]	2.93 (±0.08)	0.29	0.26	0.99
ICB-9 (this study)	1200	34	0.5	5.57E-11	5.15E-06	50.26 (±0.72)	1.03 (±0.06)	13.8 (±0.32)	6.04 (±0.40)	8.78 (±0.24)	11.88 (±0.32)	1.2 (±0.0.16)	0.03 (±0.02)	3.1 (±0.4) [2]	0.1 (±0.02) *	3.25 (±0.08)	0.29	0.25	0.99
ICB-10 (this study)	1200	29	0.5	5.50E-11	5.11E-06	49.34 (±1.42)	1.01 (±0.06)	12.71 (±0.40)	6.52 (±0.28)	9.34 (±0.34)	11.81 (±0.36)	0.7 (±0.18)	0.02 (±0.02)	3.18 (±0.09) [1]	0.1 (±0.02) [1]	3.37 (±0.08)	0.29	0.25	0.99
AgI/Cl-050 (Thomas and Wood 2021) modified	1200	30	0.5	2.29E-09	4.37E-05	50.52 (±0.61)	1.01 (±0.07)	14.63 (±0.28)	8.24 (±0.15)	8.67 (±0.15)	12.02 (±0.18)	1.17 (±0.06)	0	0	0.1 (±0.02) *	2.78 (±0.1)			

[1] Measured by SIMS
[2] Estimated from EPMA analysis
* Estimated based on CO_2 saturation

numbers in parentheses are analytical uncertainties of two standard deviations of analysis.

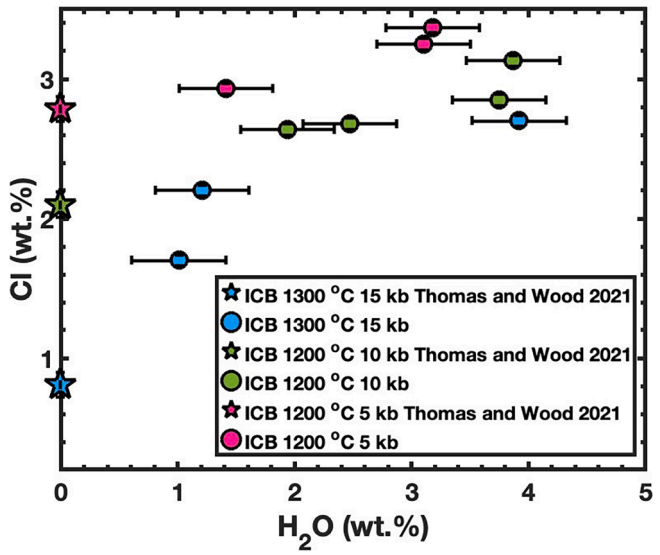

Fig. 1. Plot of the H_2O and Cl contents of the melt in hydrous experiments (circles) from this study and three anhydrous experiments (squares) of Thomas and Wood (2021) recalculated for the same temperature and chlorine fugacity as the experiments in this study. The error bars are one standard deviation for both Cl and H_2O.

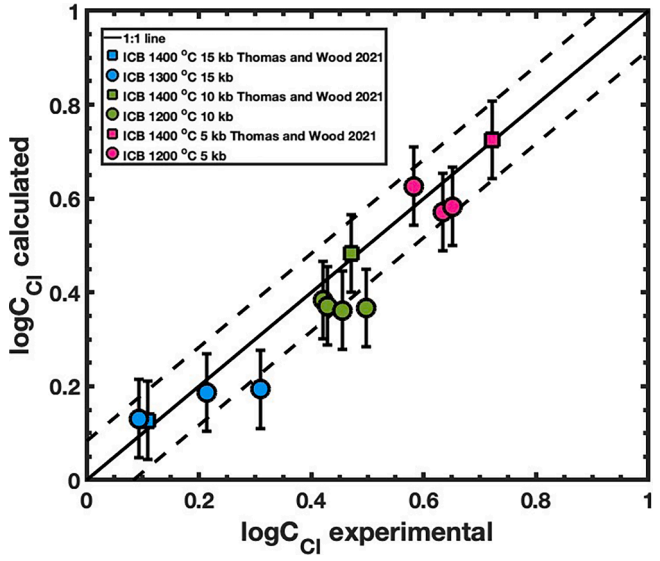

Fig. 2. Logarithm of chloride capacity calculated using equation (7) without water being considered in the sum of mol fractions ie compositions were recalculated on an anhydrous basis. The dashed lines are +/- 1 standard error of the fit ($\sigma_M = 0.083$).

which is, within uncertainty, identical to equation (7):

$$logC_{Cl} = 1.492 + (4331X_{Ca} - 3508X_{Si} + 2440X_{Fe} - 3921X_K - 741P)/T. \quad (8)$$

$R^2 = 0.963$; standard error = 0.083 for 68 % confidence interval.

Despite water having clear influence on chlorine solubility (Fig. 1) the term in $HO_{0.5}$ was found not to be significant at the minimum level ($\alpha = 0.05$). This means that the principal effect of water is that it dilutes the effects of the other cations on chloride capacity rather than itself having a strong impact on chlorine content. Water can thus be considered to be an ideal diluent at concentrations < 4 wt%. Fig. 4 shows experimental measurements of the logarithm of chloride capacity (log (C_{Cl}) experimental) plotted versus calculated values from our fit equation (8) (log(C_{Cl}) calculated) under the assumption that $HO_{0.5}$ is a simple

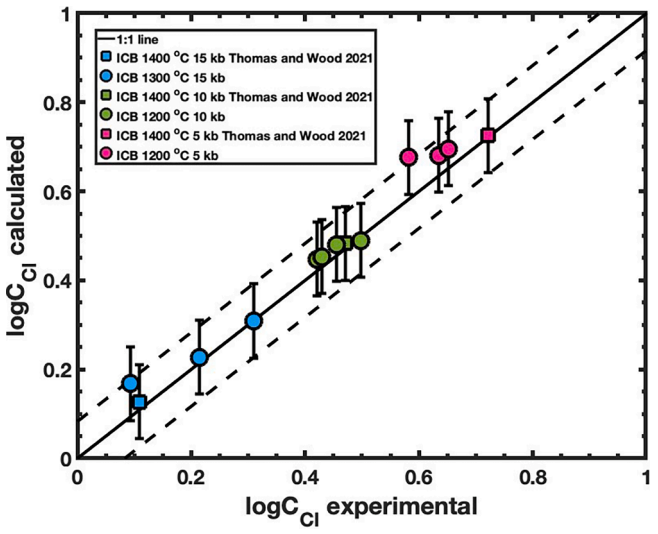

Fig. 3. Logarithm of chloride capacity calculated with water being treated as an ideal diluent using equation (7). The dashed lines are +/- 1 standard error of the fit ($\sigma_M = 0.083$).

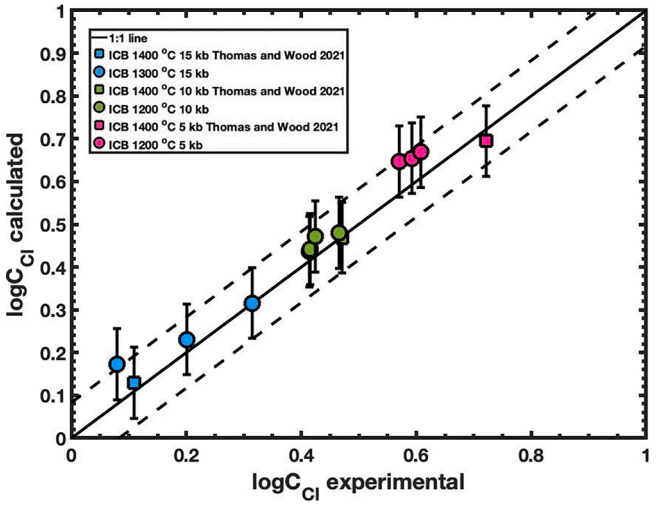

Fig. 4. Logarithm of chloride capacity calculated with water being treated as an ideal diluent using our new model (equation (8) and our experimental data (X-axis). The dashed lines are one standard error of the fit ($\sigma_M = 0.083$).

diluent. As can be seen, agreement is excellent, confirming our conclusion from Fig. 3. A further illustration of the fit is given by Fig. 5 which shows measured chlorine content of the melt (X-axis) and chlorine content calculated using chloride capacity equations (3) and (8) (Y-axis).

When considering the applicability of our chloride capacity equation (8), it should be remembered that this is not just a fit to our 10 hydrous data points, but to 70 data, comprising 60 anhydrous and 10 hydrous results. These encompass pressures from 0.5 to 2 GPa, temperatures of 1200 to 1500 °C and 25 different natural bulk compositions. The latter exhibit ranges from 40 to 75 wt% SiO_2, 5 to 21 % Al_2O_3, 0 to 18 % FeO, 0 to 23 % MgO, 0 to 22 % CaO and 0 to 9 % Na_2O (Thomas and Wood, 2023 Table 1). We are thus confident that equation (8) is applicable to virtually all natural compositions containing up to the 4 wt% H_2O we have dissolved in the basalt of our study.

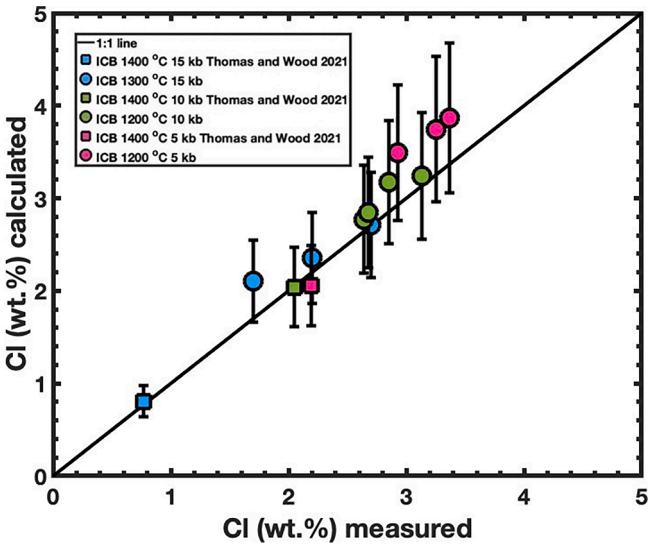

Fig. 5. Measured chlorine content in our experiments (x-axis) and chlorine content calculated using equations (3) and (8). The error bars are propagated errors of the fit.

5. Discussion

5.1. NaCl activity in silicate melt

Chlorine is a major ligand for the transport of economically important metals in hydrothermal fluids and is charge-balanced in these fluids by cations such as H^+ and Ca^{2+} but most significantly by Na^+. This observation leads to the NaCl concentration in the fluid being regarded as an important measure of the metal transport capacities of hydrothermal fluids (e.g., Kouzmanov and Pokrovski 2012, Blundy et al., 2021). The release of such fluids can lead to the formation of major ore deposits such as the porphyry copper deposits which are the source of 75 % of the world's copper, as well as significant amounts of gold and molybdenum (Blundy et al., 2021). In addition to hydrothermal fluids released deep in magmatic systems, direct gaseous emissions from volcanoes also contain chlorine which complexes volatile metals and enhances their release to the environment.

There have been several detailed studies of the solubility and behavior of chlorine in hydrous silicate melts (e.g., Webster 1992, Webster et al., 1999, 2015; Signorelli and Carroll, 2002, Carroll 2005, Stelling et al., 2008, Alletti et al., 2009, Balcone-Boissard et al., 2016). To bridge the gap between these studies and our model of chloride capacity we used experimental data from the literature to calculate the activity of NaCl in basaltic melts from the 2001 eruption of Etna (Stelling et al., 2008, Alletti et al., 2009). The experiments in both studies were conducted using internally heated pressure vessels (IHPV) with argon and argon–hydrogen mixtures as the pressure medium. The use of Ar-H_2 mixtures allowed the authors to control the oxygen fugacity in the sealed fluid-bearing capsules by imposing $\frac{f_{H_2}}{f_{H_2O}}$ in each run.

For each experimental data point we considered the equilibrium:

$$\underset{melt}{Na_2SiO_3} + \underset{gas}{Cl_2} = \underset{melt}{2NaCl} + \underset{melt}{SiO_2} + \underset{melt}{\frac{1}{2}O_2} \quad (9)$$

The condition of equilibrium is:

$$2\mu_{NaCl} + \mu_{SiO_2} + 0.5\mu_{O_2} = \mu_{Na_2SiO_3} + \mu_{Cl_2} \quad (10)$$

We make the following substitutions in equation (10):

$\mu = \mu^o + RTlna_i$

for NaCl and

$\mu = \mu^o + RTlnf_i$

for Cl_2 and O_2 where μ^o is the standard state chemical potential and a_i and f_i refer to activity and fugacity of component i respectively.

Rearranging the result and collecting terms yields an expression for NaCl activity:

$$2RTlna_{NaCl} = \mu^0{}_{Cl_2} - 0.5\mu^0{}_{O_2} - 2\mu^0{}_{NaCl} + \mu_{Na_2SiO_3} - \mu_{SiO_2} + RTln\frac{fCl_2}{\sqrt{fO_2}} \quad (11)$$

combining equation (11) and equation (3) yields:

$$2RTlna_{NaCl} = \mu^0{}_{Cl_2} - 0.5\mu^0{}_{O_2} - 2\mu^0{}_{NaCl} + \mu_{Na_2SiO_3} - \mu_{SiO_2} + 2RTln\frac{C_{Cl}}{Cl(wt.\%)} \quad (12)$$

We used standard states of gases Cl_2 and O_2 as pure gas at 1 bar and the temperature of interest while for the melt components standard states refer to the pure liquid at the pressure and temperature of interest. We obtained standard state chemical potentials (μ^0) for O_2 and Cl_2 at 1 bar using data from the NIST JANAF tables (Chase, 1998) while the partial molar free energies of SiO_2 and Na_2SiO_3 in the multicomponent melts at the P and T of interest (μ) were obtained from the rhyolite-MELTS 1.2.0 algorithm using MELTS for MatLab© (Ghiorso and Sack, 1995, Gualda et al., 2012, Ghiorso and Gualda, 2015, Antoshechkina and Ghiorso, 2018). For liquid NaCl we used the 1 bar free energy data from the NIST JANAF tables and adjusted it to the pressure and temperature of interest using NaCl volume data. The volume of pure molten NaCl at P and T was calculated using the thermal expansivity (Marcus, 2013b) and compressibility (Marcus, 2013a) and adjusted for the apparent partial molar volume of NaCl dissolved in the melt (details in the supplementary material). Pressure temperature, fO_2, Cl_2, and NaCl activity for each experiment including the 2 anhydrous NaCl-saturated experiments of Thomas and Wood (2023, at 1GPa/1100 °C) can be found in the supplementary material.

Activities of NaCl in basalts calculated using our approach (equation (12) were found to be slightly higher than those obtained from the Thomas and Wood (2023) equation. except for two anhydrous experiments of the latter authors in which a_{NaCl} was 1.0. In this case agreement between the 2 methods was found to be excellent. Since the Thomas and Wood equation relied heavily on data for SiO_2-rich and alkali-rich melts, however, we consider it likely that our method (eq. (12) employing the MELTS software should more closely approximate the data on hydrous mafic compositions than does the equation of Thomas and Wood (2023). We therefore modified the latter to take account of our calculations using equation (12).

In order to improve the NaCl activity model we took the data used by Thomas and Wood and added the experiments of Stelling et al. (2008) and Alletti et al. (2009), with NaCl activities determined using MELTS (for Na_2SiO_3 and SiO_2 activities) and our equation (8) for chlorine fugacity. Thomas and Wood showed from equilibrium (2) that there is a direct relationship between the compositional dependence of chloride capacity and the compositional dependence of $\log(\frac{a_{Cl^-melt}}{a_{O^{2-}}{}^{0.5}})$. Following this argument, we obtain from equation (8):

$$\log\left(\frac{a_{Cl^-melt}}{a_{O^{2-}}{}^{0.5}}\right) = \log(Cl^-) - (4331X_{Ca} - 3508X_{Si} + 2440X_{Fe} - 3921X_K)/T \quad (13)$$

We calculated the right-hand side of equation (13) for each experiment and subtracted it from the logarithm of NaCl activity:

$$\log(a_{NaCl}) - \log(\frac{a_{Cl^-melt}}{a_{O^{2-}}{}^{0.5}})$$

This combined parameter was then regressed against 1/T, P/T and

oxide mol fractions on a single cation basis. Details of the fitting procedure, uncertainties and weighting of the data can be found in the Supplementary material. The resulting equation is:

$$\log(a_{NaCl}) - \log\left(\frac{a_{Cl^- melt}}{a_{O^{2-}}^{0.5}}\right) = 0.23 + \frac{7484X_{Mg} + 4726X_{Na} + 8134X_{Fe} - 3160}{T} \quad (14)$$

With $R^2 = 0.915$ and standard error of 0.061

When combined with eq. (13) this gives:

$$\log(Cl^-) = \log(a_{NaCl}) - 0.23 - \frac{-4331X_{Ca} + 3508X_{Si} + 5694X_{Fe} + 7484X_{Mg} + 4726X_{Na} + 3921X_K - 3160}{T} \quad (15)$$

Rearranging (15) gives an equation for the activity of NaCl which is independent of the fugacities of both Cl_2 and O_2:

$$\log(a_{NaCl}) = \log(Cl^-) + 0.23 + \frac{-4331X_{Ca} + 3508X_{Si} + 5694X_{Fe} + 7484X_{Mg} + 4726X_{Na} + 3921X_K - 3160}{T} \quad (16)$$

Fig. 6 shows a comparison of the activity of NaCl calculated for the experiments of Stelling et al., (2008) and Alletti et al., (2009) using our new model (equation (16) with values derived from MELTS combined with our chlorine fugacities. We show both the data used in the fit to create equation (16) (circles) and test data from Stelling et al. (2008), which was not used in the fit (diamonds) and was set aside to test the validity of the fit. Either method of calculation allows us to calculate NaCl activity in both experiments and natural melts (e.g., melt inclusions) where chlorine and oxygen fugacities were not specifically controlled. As can be seen agreement between the 2 methods is generally good but, because of the uncertainties in compositions of the chlorides used to saturate melts in NaCl (equation (16) we believe that, currently, the method in which chloride capacity is combined with activities from MELTS (equation (12) is more reliable for basaltic compositions. In Supplementary Material we provide a MatLab script which enables the user to calculate both chloride capacity and NaCl activity from melt compositions. We also provide a spreadsheet for the calculation of chloride capacities and NaCl activities in basaltic melts using equations (8) and (16) (ChlorCalc 2.0).

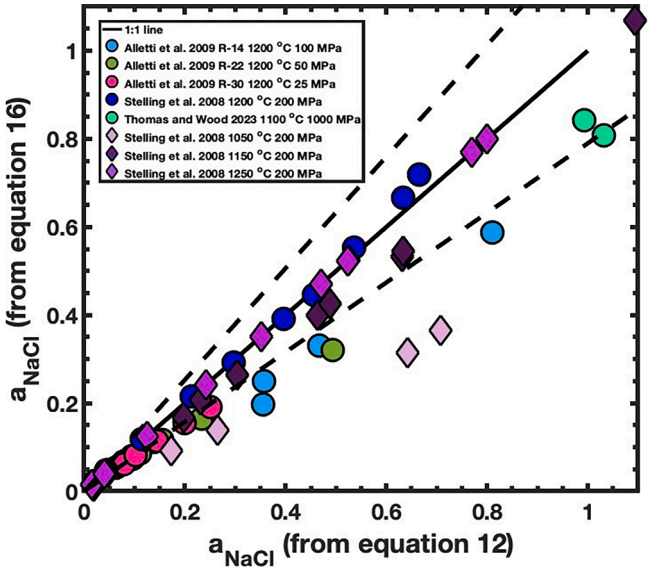

Fig. 6. Comparison of NaCl activities in experiments of Stelling et al. (2008) and Alletti et al. (2009) calculated using our model equation (16) with data generated by combining our chlorine fugacity data with Na_2SiO_3 and SiO_2 activities from MELTS (eq.12). H_2O was treated as a simple ideal diluent in the calculation of equation (16). The dashed lines are the standard error of the fit to CCl combined with the standard error of the fit to NaCl activity ($\sigma_M = \sqrt{(0.083^2 + 0.061^2)}$.) Circles are data that were used to create equation (16) and diamonds are test data not used in the fitting.

5.2. NaCl activity in natural melts

In order to explore the behaviour of NaCl in a natural basaltic system we used a set of measurements of the compositions of melt inclusions and matrix glasses from the 2002–2003 eruption of Etna presented in Spilliaert et al. (2006). The basalts produced in this highly explosive eruption were amongst the most primitive ones of the last 300 years and are very rich in volatile elements with an average H_2O content of 3.4 ±

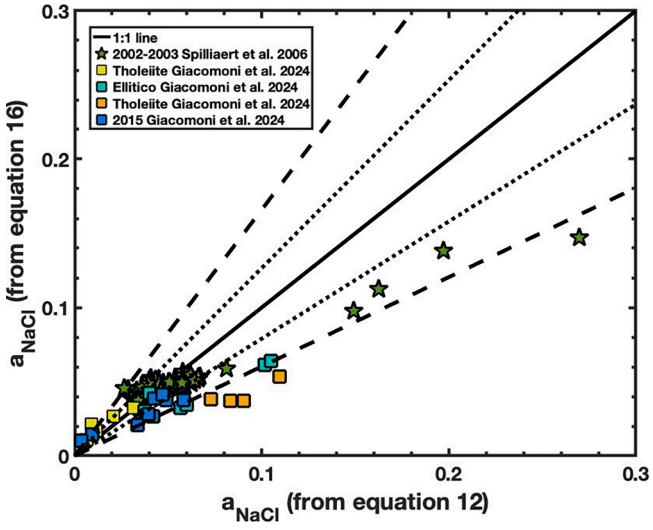

Fig. 7. NaCl activities in melt inclusions from 2002 to 2003 eruption of Etna based on the dataset presented in Spilliaert et al. (2006) and Giacomoni et al., (2024). X-axis is NaCl activity calculated using equation (12) (based on f_{Cl2} and MELTS activities) and Y-axis is NaCl activity calculated using equation (16). Pressure estimated from fluid saturation pressures, temperature assumed to be 1250 °C. The dotted lines are the standard error of the fit to CCl combined with the standard error of the fit to NaCl activity. The dashed lines are two standard errors of the fit. Two standard errors were used in an attempt to accommodate the uncertainty in composition and calculated entrapment pressures of the melt inclusions.

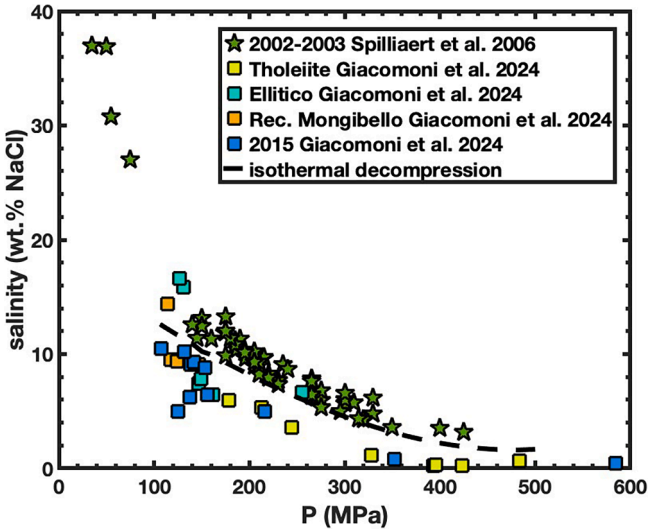

Fig. 8. Evolution of salinity (wt. % NaCl, from activity calculated using eq. (16) of the fluid in equilibrium with the melt with decreasing pressure of entrapment for the melt inclusions from different eruptions of Etna volcano (Spilliaert et al. 2006, Giacomoni et al. 2024) together with an isothermal decompression path (1250 °C, starting Cl content of 1500 ppm).

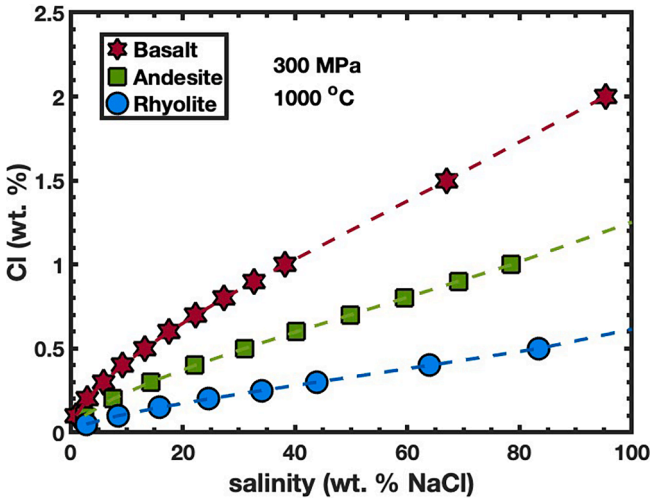

Fig. 9. Calculated salinities of fluids in equilibrium with different melts at 300 MPa and 1000 °C. The compositions of the melts (Table 3) are Icelandic basalt from Reykjanes Ridge, Iceland (Norris and Wood, 2017; Thomas and Wood, 2021, 2023; this study), andesite (Carmichael et al., 1974), and rhyolite from Uturuncu volcano, Bolivia (Muir et al., 2014). Note that the effects of increasing Na_2O, K_2O and SiO_2 combined with decreasing MgO, CaO and FeO on going from basalt to rhyolite, greatly decrease the solubility of NaCl. This leads to substantially increasing salinities of the coexisting fluids.

0.2 wt% (Spilliaert et al., 2006). To calculate the NaCl activity we used the pressure estimates of Spilliaert et al. (2006) who assumed volatile saturation and used VolatileCalc (Newmann and Lowenstern, 2002) to estimate the depth of melt entrapment. We also used a set of melt inclusion compositions from the Etna sub-alkaline and alkaline magmatic suites (Giacomoni et al. (2024) to expand our dataset to other Etna eruptions. We used both equation (16) and the MELTS/fCl_2 method (eq. (12) to calculate NaCl activity in the melt inclusions from the data of Spilliaert et al., (2006). Fig. 7 shows the results of these calculations at an assumed entrapment temperature of 1250 °C and indicates that the trapped melts have NaCl activities from close to 0 up to a maximum of about 0.26. These values may be used to estimate the compositions of H_2O-NaCl fluids with which the melts would be in equilibrium.

We used the expression of Aranovich and Newton (1996) to convert activities of NaCl in the melt inclusions to mol fractions of NaCl in coexisting aqueous fluids using eq. (16). In this calculation, for simplicity, we did not consider any chloride species other than NaCl. These were converted to salinities and are shown as a function of entrapment pressure in Fig. 8. As can be seen, the salinity of aqueous fluid coexisting with the melt increases strongly as pressure is reduced. This is due to a combination of two effects. Firstly, NaCl is released from the melt more slowly than H_2O during pressure release because the NaCl/H_2O ratio of the fluid is lower than that of the melt. This means that NaCl/H_2O of the melt increases as the pressure drops. We illustrate this effect by calculated isothermal (1250 °C) decompression paths on Fig. 8. The second effect is the increasing activity of NaCl in the melt as fractional crystallisation progresses. Fractionation leads to increasing Na_2O, K_2O and SiO_2 and decreasing CaO in the melt. As can be seen from equation (16) and Fig. 8, these effects all lead to increases in the activity of NaCl.

In order to illustrate the principal effect of decompression we calculated the isothermal, decompression path of a melt with the composition of the most primitive melt inclusion from the 2002–2003 eruption of Etna at an assumed initial Cl content of 1500 ppm. We decompressed from 500 to 100 MPa with a step of 10 MPa assuming that the melt is water saturated at each step. At each step appropriate amounts of water and NaCl were removed from the melt without extraction of other elements. We emphasize that this calculation is illustrative and is not a quantitative model of basalt decompression at Etna. In addition, for part of the diagram the NaCl-H_2O activity model of Aranovich and Newton has been extrapolated below 200 MPa by assuming that the relationships at 200 MPa also hold at lower pressure. The water content at saturation at each pressure was calculated using VolatileCalc (Newmann and Lowenstern, 2002) but we were unable to add the effects of fractional crystallisation because there is no direct connection between the most primitive and most evolved melts. Fig. 8 shows nevertheless that an isothermal, isochemical decompression path mirrors that of the Etna melt inclusions reasonably well.

In order to further illustrate the effect of composition on NaCl activity we calculated the salinities of fluids in equilibrium with water-saturated basalt, andesite and rhyolite (Fig. 9) at 1000 °C and pressure of 300 MPa. For this calculation we used the major element concentrations given in Table 3 combined with chloride capacities from equation (8) and chemical potentials of Na_2SiO_3 and SiO_2 from rhyolite-MELTS (eq. (12). NaCl activities were converted to fluid salinities using the equations of Aranovich and Newton (1996). As can be seen in Fig. 9 the salinity at constant chlorine content increases substantially with increasing silica content from basalt to rhyolite. We noted this effect in the melt inclusions from Etna. Increasing Na_2O, K_2O and SiO_2 contents together with decreasing CaO combine to increase NaCl activity and hence to increase the salinities of fluids coexisting with the melt. The salinity of a fluid in equilibrium with rhyolite, for example, at 300 MPa/1000 °C is ~ 7 times the salinity of fluid in equilibrium with a basalt having the same chlorine content (Fig. 9). In order to release fluid containing 35 wt% NaCl at 300 MPa, in the range of the fertile hypersaline fluids forming porphyry copper deposits (Bodnar et al. 2014) the rhyolite would contain ~ 2000 ppm Cl at 300 MPa (Fig. 9) and ~ 1200 ppm Cl at 200 MPa.

Table 3
Compositions of basalt, andesite and rhyolite used for the calculations resulting in Fig. 9.

	SiO2	TiO2	Al2O3	MnO	MgO	FeO	CaO	Na2O	K2O	P2O5	sum
basalt	50.76	1.02	15.32		9.19	9.61	12.26	2.01			100.17
andesite	62.85	0.62	18.30		3.49	4.01	6.89	3.37	1.04		100.57
rhyolite	75.22	0.29	13.53	0.05	0.22	1.04	0.77	2.18	6.60	0.08	99.98

6. Conclusions

This study was aimed at determining the effects of H_2O on the solubility and behaviour of chlorine in basaltic melts at high temperatures and pressures. Starting materials were based on the composition of a natural anhydrous basalt which had been used in earlier work (Thomas and Wood, 2021) with water being added as $Al(OH)_3$ in 3 increments.

Experiments were performed in graphite capsules sealed inside welded Pt capsules with a predominantly C-O atmosphere. This combination controlled oxygen fugacity close to the C-CO-CO_2 buffer. Chlorine fugacity was controlled using liquid Ag in equilibrium with a liquid AgI-AgCl melt of known Cl/(Cl + I) ratio.

Experiments were performed at 0.5–1.5GPa and 1200–1300 °C. In all series of experiments there is a clear increase in Cl contents of the melts as H_2O content is increased from 0 to 4 wt%. Although these increases suggest a major effect of H_2O on Cl solubility, we find that H_2O can actually be treated as a "neutral" or "ideal" diluent. This conclusion comes from the fact that the chloride capacity model of Thomas and Wood (2023), based solely on anhydrous experiments, agrees very well with our data on hydrous compositions under the assumption that H_2O is a "neutral" diluent. What this means is that H_2O ($HO_{0.5}$ on a single cation basis) acts solely to dilute the effects of SiO_2, CaO and other cations on chloride capacity by reducing their mole fractions.

Given this surprising agreement with the anhydrous data we wished to combine our results with those of Thomas and Wood (2021,2023) to generate a slightly improved fit. This first necessitated making a small correction to oxygen fugacities for the C-CO-CO_2 buffer at 0.5GPa in the Thomas-Wood database. We did this using an MRK equation of state for the gas species. Fitting the chlorine data using stepwise linear regression and excluding non-statistically significant terms led to for chloride capacity C_{Cl}:

$$logC_{Cl} = 1.492 + \frac{4331X_{Ca} - 3508X_{Si} + 2440X_{Fe} - 3921X_K - 741P}{T}$$

The significant terms and their magnitudes are virtually identical to those obtained by Thomas and Wood (2023). Furthermore, our new fit confirms the initial observation that the $HO_{0.5}$ fit parameter is not significant and that water acts as a simple diluent up to at least 4 wt%.

We used our chloride capacity equation to calculate the activity of NaCl in experimentally-produced hydrous basalts of known chlorine content. The method involved combining chloride capacities with Na_2SiO_3 and SiO_2 activities derived from the Rhyolite-MELTS program for the experimental melts. The results for NaCl activity were found to be in reasonably good agreement with values obtained from the Thomas and Wood (2023) equation for NaCl activity, although the "chloride capacity plus MELTS" approach generally produces higher NaCl activities. We suggest that this is due to the significant compositional differences between the calibration data used by Thomas and Wood, which are predominantly on SiO_2, Na_2O and K_2O- rich compositions and the experimental basaltic melts which are SiO_2-poor and CaO-rich. We present a revised simple equation for NaCl activity, largely based on chloride capacities and Rhyolite-MELTS activities of Na_2SiO_3 and SiO_2 which is more applicable to basaltic melts than the Thomas-Wood version.

We used the estimated activities of NaCl in melt inclusions from Mt. Etna to calculate the salinities of the fluids which would be in equilibrium with the melts. This calculation converted from NaCl activity to NaCl concentration using the activity-composition relations on the join NaCl-H_2O measured by Aranovich and Newton (1996). We found that the calculated salinities of the fluids increase with decreasing trapping pressure from ~ 1 wt% NaCl at 500 MPa to ~ 50 % NaCl at 50 MPa (Fig. 7). This is due to a combination of two effects. Firstly, NaCl is released from the melt more slowly than H_2O which means that NaCl/H_2O of the melt increases as the pressure drops. The second effect is the increasing activity of NaCl in the melt as fractional crystallisation progresses. Fractionation leads to increasing Na_2O, K_2O and SiO_2 and decreasing CaO in the melt and these effects all lead to increases in the activity of NaCl.

CRediT authorship contribution statement

Monika K. Rusiecka: Writing – review & editing, Writing – original draft, Software, Investigation. **Bernard J. Wood:** Writing – review & editing, Validation, Funding acquisition.

Data availability

The data that support the findings of this study as well as MatLab script that can be used to calculate chloride capacity and NaCl activity in melt inclusions (along with an input file) are openly available through the Oxford University Research Archive (ORA), https://doi.org/10.5287/ora-eozxmzvxp.

Declaration of competing interest

The authors declare that they have no known competing financial interests or personal relationships that could have appeared to influence the work reported in this paper.

Acknowledgements

The authors are thankful to Andrew Matzen for help with EPMA analyses and to Cees-Jan de Hoog for the SIMS analyses. We thank Associate Editor Fabrice Gaillard and 2 anonymous reviewers for their thorough reviews. This research was funded by UKRI grant EP/X031063/1 "VulcansFluids" awarded to BJW

Appendix A. Supplementary material

Supplementary material contains all the data used to create the figures and also contains details regarding derivations of eq. (12) and details of linear regression performed to fit equations (8) and (16). Supplementary material to this article can be found online at https://doi.org/10.1016/j.gca.2025.01.020.

References

Aiuppa, A., Baker, D.R., Webster, J.D., 2009. Halogens in volcanic systems. Chem. Geol. 263 (1–4), 1–18.
Alletti, M., Baker, D.R., Scaillet, B., Aiuppa, A., Moretti, R., Ottolini, L., 2009. Chlorine partitioning between a basaltic melt and H2O–CO2 fluids at Mount Etna. Chem. Geol. 263 (1–4), 37–50.
Alletti, M., Burgisser, A., Scaillet, B., Oppenheimer, C., 2014. Chloride partitioning and solubility in hydrous phonolites from Erebus volcano: A contribution towards a multi-component degassing model. GeoResJ 3.
Antoshechkina, P. M., & Ghiorso, M. S. (2018, December). MELTS for MATLAB: A new educational and research tool for computational thermodynamics. In AGU Fall Meeting Abstracts (Vol. 2018, pp. ED44B-23).

Aranovich, L.Y., Newton, R.C., 1996. H_2O activity in concentrated NaCl solutions at high pressures and temperatures measured by the brucite-periclase equilibrium. Contrib. Miner. Petrol. 125, 200–212.
Baasner, A., Schmidt, B.C., Webb, S.L., 2013. The effect of chlorine, fluorine and water on the viscosity of aluminosilicate melts. Chem. Geol. 357, 134–149.
Blundy, J., Mavrogenes, J., Tattitch, B., Sparks, S., Gilmer, A., 2015. Generation of porphyry copper deposits by gas–brine reaction in volcanic arcs. Nat. Geosci. 8 (3), 235–240.
Blundy, J., Afanasyev, A., Tattitch, B., Sparks, S., Melnik, O., Utkin, I., Rust, A., 2021. The economic potential of metalliferous sub-volcanic brines. R. Soc. Open Sci. 8 (6), 202192.
Brooker, R.A., Kohn, S.C., Holloway, J.R., McMillan, P.F., 2001. Structural controls on the solubility of CO_2 in silicate melts: part I: bulk solubility data. Chem. Geol. 174 (1–3), 225–239.
Bodnar R.J., Lecumberri-Sanchez P., Moncada D. and Steele-MacInnis M. (2014) Fluid Inclusions in Hydrothermal Ore Deposits. In: Holland H.D. and Turekian K.K. (eds.) Treatise on Geochemistry, Second Edition, vol. 13, pp. 119- 142. Oxford: Elsevier.
Boulliung, J., Wood, B.J., 2022. SO_2 solubility and degassing behavior in silicate melts. Geochim. Cosmochim. Acta 336, 150–164.
Boulliung, J., Wood, B.J., 2023. Sulfur oxidation state and solubility in silicate melts. Contrib. Miner. Petrol. 178 (8), 56.
Carmichael, I. S., Turner, F. J., & Verhoogen, J. (1974). Igneous petrology.
Carroll, M.R., 2005. Chlorine solubility in evolved alkaline magmas. Ann. Geophys.
Chase, M. (1998), NIST-JANAF Thermochemical Tables, 4th Edition, American Institute of Physics, -1 (Accessed March 3, 2024).
De Vivo, B., Lima, A., Webster, J.D., 2005. Volatiles in magmatic-volcanic systems. Elements 1 (1), 19–24.
Ding, S., Plank, T., Wallace, P.J., Rasmussen, D.J., 2023. Sulfur_X: A model of sulfur degassing during magma ascent. Geochem. Geophys. Geosyst. 24 (4), e2022GC010552.
Edmonds, M., Gerlach, T.M., Herd, R.A., 2009. Halogen degassing during ascent and eruption of water-poor basaltic magma. Chem. Geol. 263 (1–4), 122–130.
Filiberto, J., Treiman, A.H., 2009. The effect of chlorine on the liquidus of basalt: First results and implications for basalt genesis on Mars and Earth. Chem. Geol. 263 (1–4), 60–68.
Fincham, C.J.B., Richardson, F.D., 1954. The behaviour of sulphur in silicate and aluminate melts. Proc. R. Soc. Lond. A 223 (1152), 40–62.
Frantz, J.D., Eugster, H.P., 1973. Acid-base buffers; use of Ag+AgCl in the experimental control of solution equilibria at elevated pressures and temperatures. Am. J. Sci. 273 (3), 268–286.
Fuge, R., Andrews, M.J., Johnson, C.C., 1986. Chlorine and iodine, potential pathfinder elements in exploration geochemistry. Appl. Geochem. 1 (1), 111–116.
Gerlach, T.M., 2004. Volcanic sources of tropospheric ozone-depleting trace gases. Geochem. Geophys. Geosyst. 5 (9).
Gerlach, T.M., Nordlie, B.E., 1975. The COHS gaseous system; part II, temperature, atomic composition, and molecular equilibria in volcanic gases. Am. J. Sci. 275 (4), 377–394.
Ghiorso, M.S., Sack, R.O., 1995. Chemical mass transfer in magmatic processes IV. A revised and internally consistent thermodynamic model for the interpolation and extrapolation of liquid-solid equilibria in magmatic systems at elevated temperatures and pressures. Contrib. Miner. Petrol. 119, 197–212.
Ghiorso, M.S., Gualda, G.A., 2015. An H_2O–CO_2 mixed fluid saturation model compatible with rhyolite-MELTS. Contrib. Miner. Petrol. 169, 1–30.
Giacomoni, P.P., Masotta, M., Delpech, G., Lanzafame, G., Ferlito, C., Villeneuve, J., Coltorti, M., 2024. Geochemistry and volatile contents of olivine-hosted melt inclusions from Mt. Etna tholeiitic and alkaline magmatism. Contrib. Miner. Petrol. 179 (5), 47.
Gualda, G.A., Ghiorso, M.S., Lemons, R.V., Carley, T.L., 2012. Rhyolite-MELTS: a modified calibration of MELTS optimized for silica-rich, fluid-bearing magmatic systems. J. Petrol. 53 (5).
Hanfland, M., Beister, H., Syassen, K., 1989. Graphite under Pressure - Equation of State and 1st-Order Raman Modes. Phys Rev B 39 (17), 12598–12603.
Heald, E.F., Naughton, J.J., Barnes, I.L., 1963a. Chemistry of Volcanic Gases .2. Use of Equilibbrium Calculations in Interpretation of Volcanic Gas Samples. J. Geophys. Res. 68 (2), 545-+.
Hauri, E., 2002. SIMS analysis of volatiles in silicate glasses, 2: isotopes and abundances in Hawaiian melt inclusions. Chem. Geol. 183 (1–4), 115–141.
Heald, E.F., Naughton, J.J., Barnes Jr, I.L., 1963b. The chemistry of volcanic gases: 2. Use of equilibrium calculations in the interpretation of volcanic gas samples. J. Geophys. Res. 68 (2), 545–557.
Holloway, J. R. (1977). Fugacity and activity of molecular species in supercritical fluids. In Thermodynamics in Geology: Proceedings of the NATO Advanced Study Institute held in Oxford, England, September 17–27, 1976 (pp. 161-181). Dordrecht: Springer Netherlands.
Jakobsson, S., Oskarsson, N., 1994. The system CO in equilibrium with graphite at high pressure and temperature: An experimental study. Geochim. Cosmochim. Acta 58 (1), 9–17.
Kouzmanov, K., & Pokrovski, G. S. (2012). Hydrothermal controls on metal distribution in porphyry Cu (-Mo-Au) systems.
Marcus, Y., 2013a. The compressibility of molten salts. J. Chem. Thermodyn. 61, 7–10.
Marcus, Y., 2013b. Volumetric behavior of molten salts. Thermochim Acta 559, 111–116.
Marschik, R., Kendrick, M.A., 2015. Noble gas and halogen constraints on fluid sources in iron oxide-copper-gold mineralization: Mantoverde and La Candelaria, Northern Chile. Miner. Deposita 50, 357–371.
Martin, R.S., Wheeler, J.C., Ilyinskaya, E., Braban, C.F., Oppenheimer, C., 2012. The uptake of halogen (HF, HCl, HBr and HI) and nitric (HNO3) acids into acidic sulphate particles in quiescent volcanic plumes. Chem. Geol. 296, 19–25.
Millsteed, P.W., Mavrogenes, J.A., 2015. The discovery of halogens in the ores at Broken Hill, NSW - Economic implications of sulfide melting, 1 p. Society of Economic Geologists, Canberra, Abstract.
Moore, W.J., Nash, J.T., 1974. Alteration and fluid inclusion studies of the porphyry copper ore body at Bingham, Utah. Economic Geol. 69 (5), 631–645.
Moore, G., Vennemann, T., Carmichael, I.S.E., 1998. An empirical model for the solubility of H_2O in magmas to 3 kilobars. Am. Mineral. 83 (1–2), 36–42.
Muir, D.D., Blundy, J.D., Rust, A.C., Hickey, J., 2014. Experimental constraints on dacite pre-eruptive magma storage conditions beneath Uturuncu volcano. J. Petrol. 55 (4), 749–767.
Nash, J.T., 1976. Fluid-Inclusion Petrology - Data from Porphyry Copper Deposits and Applications to Exploration. Professional Paper 907-D.
Newman, S., Lowenstern, J.B., 2002. VolatileCalc: a silicate melt–H_2O–CO_2 solution model written in Visual Basic for excel. Comput. Geosci. 28 (5), 597–604.
Norris, C.A., Wood, B.J., 2017. Earth's volatile contents established by melting and vaporization. Nature 549 (7673), 507–510.
O'Neill, H.S.C., Mavrogenes, J.A., 2002. The sulfide capacity and the sulfur content at sulfide saturation of silicate melts at 1400 C and 1 bar. J. Petrol. 43 (6), 1049–1087.
O'Neill, H.S.C., Mavrogenes, J.A., 2022. The sulfate capacities of silicate melts. Geochim. Cosmochim. Acta 334, 368–382.
Palme, H., O'Neill, H.S.T.C., 2013. Cosmochemical estimates of mantle composition. In: The Mantle and Core. Elsevier, pp. 1–39.
Pyle, D.M., Mather, T.A., 2009. Halogens in igneous processes and their fluxes to the atmosphere and oceans from volcanic activity: A review. Chem. Geol. 263 (1–4), 110–121.
Sandland, T.O., Du, L.S., Stebbins, J.F., Webster, J.D., 2004. Structure of Cl-containing silicate and aluminosilicate glasses: A 35Cl MAS-NMR study. Geochim. Cosmochim. Acta 68 (24), 5059–5069.
Scholtysik, R., Canil, D., 2021. The effects of S, Cl and oxygen fugacity on the sublimation of volatile trace metals degassed from silicate melts with implications for volcanic emissions. Geochim. Cosmochim. Acta 301, 141–157.
Shishkina, T.A., Botcharnikov, R.E., Holtz, F., Almeev, R.R., Portnyagin, M.V., 2010. Solubility of H_2O-and CO_2-bearing fluids in tholeiitic basalts at pressures up to 500 MPa. Chem. Geol. 277 (1–2), 115–125.
Signorelli, S., Carroll, M.R., 2000. Solubility and fluid-melt partitioning of Cl in hydrous phonolitic melts. Geochim. Cosmochim. Acta 64 (16), 2851–2862.
Spilliaert, N., Allard, P., Métrich, N., Sobolev, A.V., 2006. Melt inclusion record of the conditions of ascent, degassing, and extrusion of volatile-rich alkali basalt during the powerful 2002 flank eruption of Mount Etna (Italy). J. Geophys. Res. Solid Earth 111 (B4).
Stanley, B.D., Hirschmann, M.M., Withers, A.C., 2011. CO_2 solubility in Martian basalts and Martian atmospheric evolution. Geochim. Cosmochim. Acta 75 (20), 5987–6003.
Stebbins, J.F., Du, L.S., 2002. Chloride ion sites in silicate and aluminosilicate glasses: A preliminary study by 35Cl solid-state NMR. Am. Mineral. 87 (2–3), 359–363.
Stelling, J., Botcharnikov, R.E., Beermann, O., Nowak, M., 2008. Solubility of H_2O-and chlorine-bearing fluids in basaltic melt of Mount Etna at T= 1050–1250 ^oC and P=200 MPa. Chem. Geol. 256 (3–4), 102–110.
Symonds, R.B., Rose, W.I., Bluth, G.J., Gerlach, T.M., 1994. Volcanic-gas studies: methods, results, and applications. Rev. Mineral. 30, 1.
Thomas, R.W., Wood, B.J., 2021. The chemical behaviour of chlorine in silicate melts. Geochim. Cosmochim. Acta 294, 28–42.
Thomas, R.W., Wood, B.J., 2023. The effect of composition on chlorine solubility and behavior in silicate melts. Am. Mineral. 108 (5), 814–825.
von Glasow, R., Bobrowski, N., Kern, C., 2009. The effects of volcanic eruptions on atmospheric chemistry. Chem. Geol. 263 (1–4), 131–142.
Webster, J.D., 1992. Water solubility and chlorine partitioning in Cl-rich granitic systems: effects of melt composition at 2 kbar and 800 C. Geochim. Cosmochim. Acta 56 (2), 679–687.
Webster, J.D., Kinzler, R.J., Mathez, E.A., 1999. Chloride and water solubility in basalt and andesite melts and implications for magmatic degassing. Geochim. Cosmochim. Acta 63 (5), 729–738.
Webster, J.D., De Vivo, B., 2002. Experimental and modeled solubilities of chlorine in aluminosilicate melts, consequences of magma evolution, and implications for exsolution of hydrous chloride melt at Mt. Somma-Vesuvius. Am. Mineral. 87 (8–9), 1046–1061.
Webster, J.D., Vetere, F., Botcharnikov, R.E., Goldoff, B., McBirney, A., Doherty, A.L., 2015. Experimental and modeled chlorine solubilities in aluminosilicate melts at 1 to 7000 bars and 700 to 1250 C: Applications to magmas of Augustine Volcano, Alaska. Am. Mineral. 100 (2–3), 522–535.
Webster, J.D., Baker, D.R., Aiuppa, A., 2018. Halogens in mafic and intermediate-silica content magmas. The Role of Halogens in Terrestrial and Extraterrestrial Geochemical Processes: Surface, Crust, and Mantle 307–430.
Zhao, L., Tang, J., Zhou, M., Shen, K., 2022. A review of the coefficient of thermal expansion and thermal conductivity of graphite. New Carbon Mater 37 (3), 544–555.
Zimova, M., Webb, S., 2006. The effect of chlorine on the viscosity of Na_2O-Fe_2O_3-Al_2O_3-SiO_2 melts. Am. Mineral. 91 (2–3), 344–352.